Science of the Total Environment 729 (2020) 138639

Contents lists available at ScienceDirect

Science of the Total Environment

journal homepage: www.elsevier.com/locate/scitotenv

Fossil fuel CO_2 traced by radiocarbon in fifteen Chinese cities

Weijian Zhou [a,b,c,*,1], Zhenchuan Niu [a,b,c,1], Shugang Wu [a,c], Xiaohu Xiong [a,c], Yaoyao Hou [a,c], Peng Wang [a,c], Tian Feng [a,c], Peng Cheng [a,d], Hua Du [a,c], Xuefeng Lu [a,c], Zhisheng An [a,b,d], G.S. Burr [a,c], Yizhi Zhu [a,c]

[a] State Key Laboratory of Loess and Quaternary Geology, CAS Center for Excellence in Quaternary Science and Global Change, Institute of Earth Environment, Chinese Academy of Sciences, Xi'an 710061, China
[b] Open Studio for Oceanic-Continental Climate and Environment Changes, Pilot National Laboratory for Marine Science and Technology, Qingdao 266061, China
[c] Shaanxi Provincial Key Laboratory of Accelerator Mass Spectrometry Technology and Application, Joint Xi'an AMS Center between IEECAS and Xi'an Jiaotong University, Xi'an 710061, China
[d] Interdisciplinary Research Center of Earth Science Frontier, Beijing Normal University, Beijing 100875, China

HIGHLIGHTS

- China has dual problems-CO_2 emissions reductions and air pollution mitigation.
- CO_{2ff} in Xi'an dropped after implementation of a 2013 pollution prevention plan.
- Case study showed that CO_{2ff} in Xi'an was mainly from local coal combustion.
- CO_{2ff} in January was significantly higher than that in July in most cities.
- Positive correlations were found between CO_{2ff} and $PM_{2.5}$ in Chinese cities.

GRAPHICAL ABSTRACT

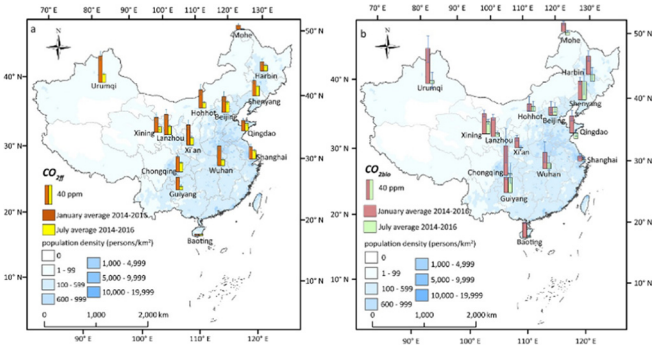

ARTICLE INFO

Article history:
Received 24 January 2020
Received in revised form 9 April 2020
Accepted 9 April 2020
Available online 15 April 2020

Editor: Mae Sexauer Gustin

Keywords:
Fossil fuel CO_2
Radiocarbon
Cities
Carbon reduction
$PM_{2.5}$

ABSTRACT

China is an important fossil fuel CO_2 (CO_{2ff}) emitter and the international community is thus concerned with quantifying reductions in Chinese carbon emissions in the recent past. Compared to traditional statistical method, radiocarbon (^{14}C) offers a different approach to quantify atmospheric CO_2 derived from fossil fuel emissions. Here, we carry out a multi-year (2011–2016) CO_{2ff} tracing by ^{14}C in Xi'an, and a three-year (2014–2016) CO_{2ff} tracing in 15 Chinese cities. The Xi'an results show that average CO_{2ff} concentrations fell 35.9 ± 6.6% from 2014– 2016, compared to 2011–2013, and the timing of this decrease coincides with the implementation of nationwide carbon reduction measures in China, known as the *Action Plan on Prevention and Control of Air Pollution*. A WRF-Chem forward modeling simulation reveals that the CO_{2ff} in Xi'an is mainly derived from local sources, and a source apportionment combined stable-carbon isotope showed that the CO_{2ff} in this city is dominated by coal combustion (72.6 ± 10.4%). Strong CO_{2ff} differences are found between January and July in most Chinese cities. High CO_{2ff} concentrations often correspond to severe haze episodes and there are generally positive correlations between CO_{2ff} and fine particulate ($PM_{2.5}$) concentrations. Our study provides scientific data to understand the effects of CO_{2ff} reduction strategies in China that can be applied to other countries as well.

* Corresponding author at: State Key Laboratory of Loess and Quaternary Geology, CAS Center for Excellence in Quaternary Science and Global Change, Institute of Earth Environment, Chinese Academy of Sciences, Xi'an 710061, China.
E-mail address: weijian@loess.llqg.ac.cn (W. Zhou).
[1] These authors contributed equally to this work.

https://doi.org/10.1016/j.scitotenv.2020.138639
0048-9697/

1. Introduction

With rapid economic growth in recent decades, about 57.4% of the Chinese population now lives in cities (NBSC, 2017), and the urban population is expected to reach about 75% in 2040 (UN, 2014). This accelerates the need to address the dual problems of carbon emissions reductions and air pollution mitigation. China is now the world's largest CO_2 emitter (Boden et al., 2013), accounting for approximate 23% of total global emissions (BP, 2018). The magnitude of CO_2 emissions in China is often estimated by statistical data, but this approach can incur large uncertainties (Liu et al., 2015). Other independent and objective methods are needed to study fossil fuel- derived CO_2 (CO_{2ff}).

Radiocarbon (^{14}C) is a unique tracer for the identification of atmospheric CO_2 emitted from fossil fuels, because ^{14}C is depleted in fossil fuels due to their great age, in comparison with the ^{14}C half-life of 5730 ± 40 years (Godwin, 1962). The marked difference in ^{14}C content can be used to distinguish between atmospheric CO_{2ff} and CO_2 from other sources (Levin et al., 2003; Turnbull et al., 2006). Recently, ^{14}C was used to determine the spatial-temporal variations in atmospheric CO_{2ff} concentrations in several Chinese cities (Xi et al., 2011; Zhou et al., 2014; Niu et al., 2016); however, these studies are limited in terms of city coverage, and a lack of long-term (multi-year) and large-scale observations makes it difficult to integrate these data to determine the overall characteristics or trend of atmospheric CO_{2ff} in China.

High fine particulate ($PM_{2.5}$) concentrations have adverse effects on human health. For example, a study in Guangzhou, China, covering statistics collected over 52 years, showed a significant relationship, with a 7-year lag, between air quality and the mortality related with lung cancers (Tie et al., 2009). To control air pollution, the Chinese government instituted the "Action Plan on Prevention and Control of Air Pollution" (henceforth, the *Action plan*) in September 2013 (Chinese State Council, 2013). Although the *Action plan* aimed to decrease atmospheric particulate matter concentrations, these measures also have influenced fossil-fuel emissions. For example, one of the measures implemented reduces the coal share in the energy mix, and promotes a clean coal utilization strategy, as coal combustion emits more CO_2 to produce the same unit of heat as other energy sources. The work was designed to obtain the characteristics and sources of CO_{2ff}, and the influence of the *Action plan* on CO_{2ff} concentrations in cities where about 80% of CO_{2ff} emissions in China are concentrated (Dhakal, 2009). In this paper, a multi-year atmospheric CO_{2ff} tracing program by $\Delta^{14}C$ was reported in Xi'an. This program identified CO_{2ff} sources and transport pathways using ^{14}C, stable-carbon isotope (^{13}C), and Weather Research and Forecasting-Chemistry (WRF-Chem) modeling. This CO_{2ff} tracing was then expanded to include 15 Chinese cities for the period 2014 to 2016. Furthermore, the relationship between CO_{2ff} and $PM_{2.5}$ was explored by comparison of contemporaneous time series of both parameters from individual cities. The aim of this paper was to provide a complete picture of atmospheric CO_{2ff} in Chinese cities, and provide scientific data bearing on CO_{2ff} reduction strategies in China.

2. Methods

2.1. Sites and sampling

Air samples were collected in 15 Chinese cities and a background site from Qixianling Mountain (Fig. 1). The background site (18.70°N, 109.81°E, 290 *m* asl) is located in a forested area in Hainan Province, and is subject to minimal human disturbance. This site has been used to obtain background $\Delta^{14}CO_2$ value in our previous studies (Zhou et al., 2014). The $\Delta^{14}CO_2$ values at the Qixianling Mountain in this study are generally comparable to those at the Jungfraujoch background site in Switzerland (Hammer and Levin, 2017), and the detailed comparison is shown in Section 3.1. Therefore, the $\Delta^{14}CO_2$ data at the Qixianling Mountain were appropriate to be used as the background values. In general, two urban sites were selected in each studied city. The details of each sampling site are listed in Table S1. These sites are generally located in cultural, educational, commercial and residential areas, generally no >300 *m* from the closest air-quality monitoring station set up by the Ministry of Ecology and Environment of the People's Republic of China. The sites were generally on the building tops, but selected to be free of any modifying effects of surrounding skyscrapers. The sampling height was maintained at least 10 *m* above the ground.

For the multi-year monitoring program in Xi'an, 322 daily samplings were conducted on the roof of the building (34.23°N, 108.89°E, 10 *m* above the ground) at the Institute of Earth Environment, Chinese Academy of Sciences (IEECAS) in Xi'an from October 2011 to January 2013; 51 weekly samples were collected from February to December 2013, and 76 fortnightly samples were collected from January 2014 to December 2016. Samples were collected using a phosphoric acid solution displacement method. Detailed description of the method is discussed in Zhou et al. (2014). Briefly, a 4-l flask with an air inlet and a solution outlet, is filled with a phosphoric acid solution to prevent CO_2 dissolution, and the flask was inverted. While the acid solution flows out of the flask drop by drop, air is compressed into the flask because of the pressure gradient between the inside and outside of the flask. The flow rate can be controlled by a regulator for a predesignated sampling time.

For the CO_{2ff} tracing in the 15 studied Chinese cities, air samples were collected into 5-L aluminum foil sampling bags (Delin Gas Packing Co., Ltd., Dalian, China) using pumps at a flow rate of about 85 ml min^{-1}. The bag sampling method has been utilized in former studies (Takahashi et al., 2002; Niu et al., 2016), and imparts minimal influence (ca. 0.02 ppm) on CO_{2ff} calculations (Niu et al., 2016). One-week samples were carried out at each site generally in January and July from 2014 to 2016. The samples were collected during 14:00–16:00 (local time), when the atmospheric boundary layer is deepest and relatively well-mixed. Meteorological parameters and the nearby $PM_{2.5}$ concentrations were obtained from the China air quality online monitoring and analysis platform (China MEP, 2016) coincident with sampling.

2.2. CO_2 concentration, $\delta^{13}C$ and $\Delta^{14}C$ measurement

CO_2 concentration and $\delta^{13}C$ values were analyzed with a Picarro G2131-i CO_2 gas analyzer (Picarro Inc., USA) at a flow rate of 25 ml min^{-1}. This equipment employs a cavity ring-down spectroscopy (CRDS) technology, with high linearity, precision, and stability for CO_2 measurements. A CRDS instrument is composed of a laser, a high-finesse optical cavity, and a photodetector. Briefly, the sample air was filtered, dried in an ethanol-liquid nitrogen cold trap (−90 °C), and then introduced into a high-finesse optical cavity. $\delta^{13}C$ was determined using a 30-s moving average. Each sample was measured for 6 min, and only the average of the data from the last 4 min was used to minimize equipment instability created dead volumes when switching to a new sample. The CO_2 concentration of a sample is the sum of the $^{12}CO_2$_dry and $^{13}CO_2$_dry. The precision of the CO_2 concentrations in this study are ~0.1 ppm and $\delta^{13}C$ precision is <0.2‰. These consumed ca. 150 ml of air per sample. The ^{13}C data of samples are expressed using δ notation, relative to Vienna Pee Dee Belemnite (VPDB) on a scale defined by adopting a $\delta^{13}C$ value of +1.95‰ for NBS19-limestone (RM 8544) relative to VPDB (Coplen, 1995).

The remaining gas was first passed through a liquid nitrogen trap (−196 °C) in a vacuum system to trap CO_2 and water, and trapped water was removed with an ethanol-liquid nitrogen trap (−90 °C). A zinc-iron method was used for the graphitization of CO_2, with zinc particles and iron powder as reductant and catalyst, respectively (Slota et al., 1987). The obtained graphite (1.0–1.2 mg) was pressed into aluminum target holders for ^{14}C measurement using a 3 MV AMS instrument (HVE, the Netherlands) at the Xi'an AMS Center (Zhou et al., 2006). Standard air samples with the same treatment processing were used to determine the chemical process uncertainty of 2.3‰ (1σ) (Niu et al., 2016).

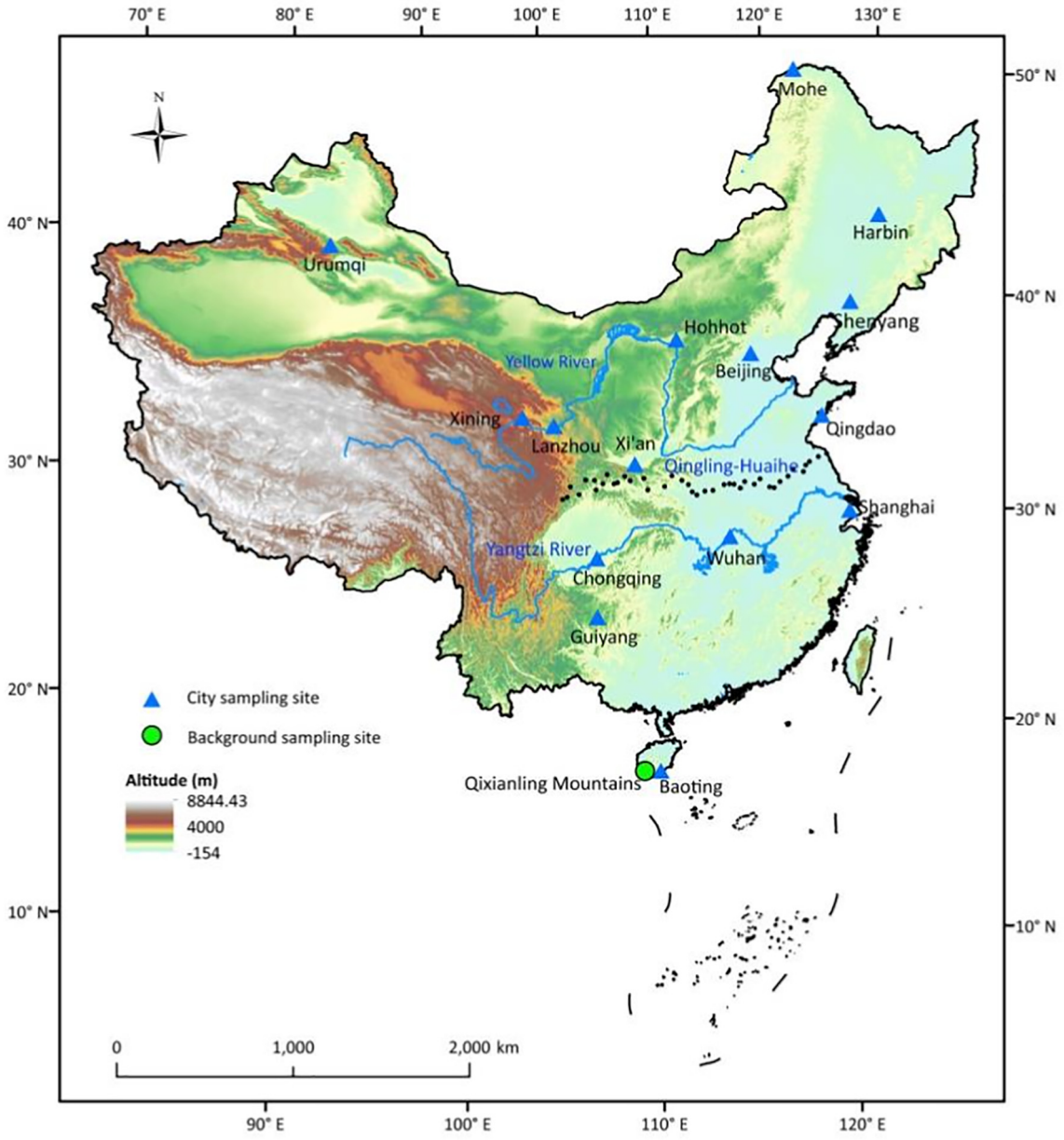

Fig. 1. Sampling sites. Blue triangles are cities and the green dot is the background site at Qixianling Mountain. Black dot line is Qinling-Huaihe line, dividing China into northern and southern regions.

The ^{14}C levels determined here are expressed as $\Delta^{14}C$ values, i.e., the per mil (‰) deviation from the absolute radiocarbon reference standard, corrected for fractionation and decay (Stuiver and Polach, 1977).

$$\Delta^{14}C = \left[\frac{C_{14}/C_{12_{SN}}}{C_{14}/C_{12_{ABS}}} - 1\right] \times 1000‰ \quad (1)$$

where $(^{14}C/^{12}C)_{SN}$ is the $^{14}C/^{12}C$ ratio of the sample normalized to a common $\delta^{13}C$ value of −25‰ and $(^{14}C/^{12}C)_{ABS}$ is the absolute radiocarbon reference standard after the fractionation and decay corrections. Background and seasonal averages of $\Delta^{14}C$ results are shown in Table 1, Table S1 and Fig. S1.

2.3. Calculation of CO_{2ff}

The observed CO_2 fraction (CO_{2obs}) is related to the mixing of atmospheric background CO_2 (CO_{2bg}), CO_{2ff} and other CO_2 (CO_{2other}) (Levin et al., 2003; Zondervan and Meijer, 1996; Turnbull et al., 2009). The $\Delta^{14}C$ values for CO_{2obs}, CO_{2bg}, CO_{2other} and CO_{2ff} are expressed as Δ_{obs}, Δ_{bg}, Δ_{other} and Δ_{ff} (−1000‰). According to mass balance equations, Eqs. (2) and (3) are obtained.

$$CO_{2obs} = CO_{2bg} + CO_{2other} + CO_{2ff} \quad (2)$$

Table 1
Atmospheric background $\Delta^{14}CO_2$ values at Qixianling Mountain (this study), and Jungfraujoch, Switzerland (Hammer and Levin, 2017).

Season	$\Delta^{14}C$ (‰) at Qixianling	$\Delta^{14}C$ (‰) at Jungfraujoch
Winter, 2014	17.3 ± 4.0	20.8 ± 2.1
Summer, 2014	23.0 ± 3.7	21.5 ± 1.2
Winter, 2015	16.3 ± 3.3	16.6 ± 1.3
Summer, 2015	21.6 ± 4.0	12.2 ± 1.3
Winter, 2016	12.8 ± 3.3	11.1 ± 1.6
Summer, 2016	16.5 ± 2.9	–

$$CO_{2obs}\,\Delta_{obs} = CO_{2bg}\,\Delta_{bg} + CO_{2other}\,\Delta_{other} + CO_{2ff}\,\Delta_{ff} \quad (3)$$

From Eqs. (2) and (3), CO_{2ff} can be calculated with the following equation:

$$CO_2ff = \frac{CO_2obs\Delta_{bg} - \Delta_a}{\Delta_{bg}} - \Delta_{ff} + \frac{CO_2other\Delta_{other} - \Delta_{bg}}{\Delta_{bg}} - \Delta_{ff} \quad (4)$$

The second term on the right-hand-side of Eq. (4) is a small correction (β) mainly from heterotrophic respiration. The CO_{2ff} correction is 0.2–0.3 ppm during the winter months and 0.4–0.8 ppm during the summer months (Turnbull et al., 2006, 2009). The minor nuclear power plants (NPPs) effect was not considered in this study, because our sampling sites are far from NPPs. CO_{2ff} corrections that resulted from NPPs are small, from −0.25 ppm over large regions to several ppm near nuclear sites (Vogel et al., 2013; Graven and Gruber, 2011).

2.4. CO_{2ff} source apportionment in Xi'an

Overall, there are three main CO_{2ff} emission sources in most Chinese cities: 1) coal combustion for heating and power generation, 2) motor vehicle exhaust, and 3) natural gas combustion (Shan et al., 2017). Since the $\delta^{13}C$ values among these fossil fuels sources are different, the measurement of $\delta^{13}C$ can be used to separate fossil fuel sources further (Clark-Thorne and Yapp, 2003; Djuricin et al., 2010; Newman et al., 2016; Pataki et al., 2003). The $\delta^{13}C$ mass balance is described by the following two equations:

First, the stable isotopic signature of local sources ($\delta^{13}C_s$) is needed to recognize. A Miller-Tans plot (Miller and Tans, 2003) was used to determine $\delta^{13}C_s$, because the method does not require a stable background composition.

$$CO_{2obs} = CO_{2bg} + CO_{2s} \quad (5)$$

$$CO_{2obs}\,\delta^{13}C_{obs} = CO_{2bg}\,\delta^{13}C_{bg} + CO_{2s}\,\delta^{13}C_s \quad (6)$$

The subscripts *obs*, *bg* and *s* represent the CO_2 concentration and $\delta^{13}C$ values of observed, background and local sources, respectively. The CO_{2bg} and $\delta^{13}C_{bg}$ values used in this study were 398.8 ppm and − 8.55‰, respectively, obtained from the Waliguan background station (GMD-ESRL, 2014). From Eqs. (5) and (6), a new equation can be derived as follows:

$$CO_{2obs}\,\delta^{13}C_{obs} - CO_{2bg}\,\delta^{13}C_{bg} = \delta^{13}C_s\,(CO_{2obs} - CO_{2bg}) \quad (7)$$

If Eq. (7) is treated as a linear function of y = ax+b type, the $\delta^{13}C_s$ is the slope (a), which can be determined by performing a linear regression analysis of our observed data and background data. Generally, $\delta^{13}C_s$ does not represent the isotopic signature of a single CO_2 source, but represents the weighted average value of different sources which contribute to atmospheric CO_2 (Miller and Tans, 2003), such as fossil fuels and biosphere sources in this study. Thus, it can be described as follows:

$$\delta^{13}C_{ff} = \left(\delta^{13}C_s - F_{bio}\,\delta^{13}C_{bio}\right)/F_{ff} \quad (8)$$

Here, F_{ff} represents the fractional contribution of fossil fuels to excess CO_2 (CO_{2ex}, subtracting the background CO_2 concentration from the total CO_2 concentration), which can be derived from the CO_{2ff}/CO_{2ex}. Considering the complexity of ecosystems and the unknown ratio for C3 and C4 plants, a value of −24.7‰ was used to represent biospheric $\delta^{13}C$, a value that is commonly used in similar studies (Bakwin et al., 1998; Lopez et al., 2013; Moore and Jacobson, 2015). Therefore, the isotopic signature of fossil fuels ($\delta^{13}C_{ff}$) can be calculated from Eq. (8).

The decomposition of $\delta^{13}Cs$ becomes counter-intuitive when fluxes of opposing sign are involved (Miller and Tans, 2003), so source apportionment was conducted only during the winter sampling period because the assimilation process of photosynthesis is rather weak and can be ignored during wintertime in Xi'an. And then the proportions of CO_2 from different fossil fuels can be calculated as follows:

$$\delta^{13}C_{coal}\,F_{coal} + \delta^{13}C_{exh}\,F_{exh} + \delta^{13}C_{ng}\,F_{ng} = \delta^{13}C_{ff} \quad (9)$$

$$F_{coal} + F_{exh} + F_{ng} = 1 \quad (10)$$

where F_{coal}, F_{exh} and F_{ng} represent the share of coal burning, vehicle exhaust and natural gas combustion, respectively. The $\delta^{13}C$ value for Chinese coal ($\delta^{13}C_{coal}$) is taken as −23.5‰ and natural gas ($\delta^{13}C_{ng}$) as −39.5‰ (Tang, 2001; Pang et al., 2016). The $\delta^{13}C$ value (−31.2‰) for vehicle exhaust ($\delta^{13}C_{exh}$) was measured in a road tunnel in Xi'an. The tunnel is situated at the First Ring road, which is one of the busiest main roads around the Xi'an city center, with a length of 900 m. Meanwhile, in order to capture adequate signatures of vehicle emissions in Xi'an, our sampling campaigns were conducted during the rush hours. All of the three sources cannot be partitioned based on the two equations. Hence, a "bottom up" method (Shan et al., 2017) was used to establish CO_2 emissions inventory at a city level. A detailed description of the emissions inventory in Xi'an is given in the Supplementary material (Table S3). The results showed that the annual average contribution of natural gas to the total emissions was 13.6% in 2014, which was used as the reference index in the source apportionment study, and then the proportions of the two other sources are determined using Eqs. (9) and (10).

2.5. Atmospheric CO_{2ff} simulation in Xi'an

2.5.1. CO_{2ff} simulation in the WRF-Chem model

A modified version of the WRF-Chem model was used to simulate CO_2 concentrations in the atmosphere. In this specific version, atmospheric total CO_2 (CO_{2a}) includes 3 components: background, fossil fuel, and other components as described in Eq. (2). Since the small bias (Eq. 4) is mainly from heterotrophic respiration (Turnbull et al., 2006, 2009), the model includes CO_2 emission rates from heterotrophic respiration (CO_{2hr}) and CO_2 absorption rates in photosynthesis (CO_{2ph}) of the terrestrial biosphere, obtained from the Global Fire Emissions Database, Version 4 (GFEDv4, Randerson et al., 2018) as described in Section 2.5.2. The CO_2 exchange of terrestrial biosphere with the atmosphere in the model (a, b) is treated as follows:

(a) Photosynthesis of the terrestrial biosphere:

$$\Delta CO_{2bg}(t) = -\frac{CO_{2bg}(t)}{CO_{2a}}(t)\cdot CO_{2ph}(t)\cdot\Delta t \quad (11)$$

$$\Delta CO_{2ff}(t) = -\frac{CO_{2ff}(t)}{CO_2a(t)}CO_{2ph}(t)\cdot\Delta t \quad (12)$$

$$\Delta CO_2other(t) = -\frac{CO_{2other}(t)}{CO_{2a}}(t)\cdot CO_{2ph}(t)\cdot\Delta t \quad (13)$$

(b) Heterotrophic respiration of the terrestrial biosphere:

$$\Delta CO_{2other}(t) = CO_{2hr}(t)\cdot\Delta t \quad (14)$$

2.5.2. Model and its configuration

We simulated wintertime atmospheric CO_2 concentrations during January 2014, and summertime concentrations in July 2012, in the Guanzhong basin. We employed a modified WRF-CHEM model (Feng et al., 2018), with a grid spacing of 6 km (150 × 150 grid cells and centered on Xi'an). We used 35 stretched vertical levels with spacing ranging from 50 *m* near the surface, to 500 *m* at 2.5 km above ground level

(a.g.l) and >1 km at altitudes above 14 km. The model employed the microphysics of Lin et al. (1983), the Mellor-Yamada-Janjic (MYJ) turbulent kinetic energy (TKE) planetary boundary layer scheme, the MYJ surface layer scheme (Janjić, 2002), the Unified Noah land-surface model (Chen and Dudhia, 2001), and the New Goddard shortwave (Chou and Suarez, 1999) and longwave (Chou et al., 2001) schemes. These configurations perform reasonably well in simulating the meteorology and airborne species in previous modeling studies in Xi'an and surrounding areas (e.g., Feng et al., 2016, 2018). Meteorological initial and boundary conditions were obtained from NCEP 1° × 1° reanalysis data. The NCEP ADP Global Surface Observational Weather Data (http://rda.ucar.edu/) in the simulation domain were assimilated in the model using the four-dimension data assimilation (FDDA) to improve the simulation of meteorological fields. The chemical initial and boundary CO_2 conditions were interpolated from the s04_v3.8 run with a 6-h time interval at Jena CarboScope (Rödenbeck et al., 2003).

The anthropogenic CO_2 inventories of Zhang et al. (2009) and Li et al. (2017) were adopted here, including industrial, power generation, residential, and transportation sources (Fig. S2a). The base year of the inventory is 2013. The CO_2 flux of the terrestrial biosphere represented as photosynthetic CO_2 and heterotrophic respired CO_2 (Fig. S2b and S2c) was interpolated from the monthly GFEDv4 data (Randerson et al., 2018). The database includes monthly and daily burned area (GFED4 - without small fires) and Emissions (monthly, daily, 3-hourly) and burned area (GFED4s-with small fires). The CASA-GFED biosphere flux sources include Net Primary Production (NPP), heterotrophic respiration (Rh), and fires (biomass burning).

2.5.3. Statistics

The mean bias (MB), the root mean square error (RMSE), and the index of agreement (IOA) are used to evaluate the model performance in simulating CO_2 concentrations (Li et al., 2011; Willmott, 1981).

$$MB = \frac{1}{N}\sum_{i=1}^{N}(P_i - O_i) \tag{15}$$

$$RMSE = \left[\frac{1}{N}\sum_{i=1}^{N}(P_i - O_i)^2\right]^{\frac{1}{2}} \tag{16}$$

$$IOA = 1 - \frac{\sum_{i=1}^{N}(P_i - O_i)^{2^N}}{\sum_{i=1}}\left(|P_i - \overline{O}| + |O_i - \overline{O}|\right)^2 \tag{17}$$

where P_i and O_i denote the simulated and observed variables, respectively. N is the total number of predictions and $\overline{O}$ is the average of observations. Dimensionless IOA has a theoretical range from 0 to 1. An IOA of 1 indicates perfect agreement between the simulation and observations.

2.5.4. Model evaluation

Temporal variations of simulated hourly CO_2 concentrations during the entire month of January 2014 are compared with observations from the IEECAS site, Xi'an, in Fig. S3. Observed CO_2 concentrations vary from about 400 ppm to nearly 600 ppm, reflecting variable CO_2 concentrations in the basin. During the study period, several episodes with high CO_2 concentrations are observed, which are also captured by the model, although some biases remain. Overall, the statistics show that the model reasonably reproduces observed CO_2 concentrations, and the IOA reaches 0.72. Fig. S4 shows the correlation between the simulated and observed CO_2 concentrations during January 2014. The Pearson correlation is about 0.55 ($p = .000$). The MB and IOA for the simulated and measured CO_2 concentrations during July 2012 are −1.3 ppm and 0.66, respectively, suggesting that the model reproduces measured CO_2 concentrations reasonably well (Feng et al., 2018).

3. Results and discussion

3.1. Atmospheric background $\Delta^{14}CO_2$

The calculation of CO_{2ff} concentrations is influenced by the choice of background site (Turnbull et al., 2009). Previous study has shown that there is a latitudinal gradient (ca. 2–5‰) in atmospheric $\Delta^{14}CO_2$ among different background sites (Levin et al., 2010). Our background site is in the far south of China at 18°N, and the $\Delta^{14}CO_2$ values at this site might be ca. 1–3‰ higher than those at the background sites located at higher latitudes, and this difference might overestimate 0.5–1.3 ppm for the CO_{2ff} calculation in cities.

As shown in Table 1, the atmospheric background $\Delta^{14}CO_2$ values at the Qixianling site in this study were generally comparable to those from the Jungfraujoch global site (Hammer and Levin, 2017), with an exception for the summer of 2015. The background $\Delta^{14}CO_2$ values at Qixianling (21.6 ± 4.0‰) in summer 2015 is higher than that at Jungfraujoch (12.2 ± 1.3‰). The long-term observations at Jungfraujoch showed that the $\Delta^{14}CO_2$ values in summer were approximately 5‰ higher than those in winter (Levin and Kromer, 2004; Levin et al., 2010, 2013), whereas the $\Delta^{14}CO_2$ value (12.2 ± 1.3‰) in summer, 2015 was lower than that (16.6 ± 1.3‰) in winter (Hammer and Levin, 2017). Therefore, the value of 21.6 ± 4.0‰ was selected as the background $\Delta^{14}CO_2$ value for the summer of 2015.

3.2. $\Delta^{14}CO_2$ and CO_{2ff} monitoring in Xi'an

A multi-year $\Delta^{14}CO_2$ monitoring program was carried out in the IEECAS in Xi'an to determine temporal variation characteristics of atmospheric CO_{2ff}. Fig. 2 shows distinct CO_{2ff} seasonal variations in Xi'an during 2011–2016, with winter CO_{2ff} peaks, and summer CO_{2ff} lows. Elevated CO_{2ff} winter concentrations correspond to periods of increased fossil fuel consumption for heating and a characteristic winter atmospheric temperature inversion (Zhou et al., 2014), which traps CO_{2ff} under the atmospheric boundary layer. An obvious reduction in CO_{2ff} can be seen in the Xi'an data as early as the summer of 2014 following the implementation of the *Action plan*. This reduction might be due to the decrease in fossil fuel consumption in this city from 12.0 million tons of standard coal in 2013 to 7.9 million tons of standard coal in 2016 (XMBS, 2017). The 2014 JJA (June July August) average CO_{2ff} concentration is 16.6 ± 4.4 ppm (1σ), as compared to the previous 2012–2013 JJA average of 30.0 ± 6.4 ppm. Summer levels continued to fall in 2015 and 2016, with an average of 13.9 ± 2.0 ppm during 2014–2016 summertime, about half the pre-*Action plan* value. Winter (DJF, December, January, February) CO_{2ff} values also fell, starting in 2014, but the winter data is more variable than the summer data (Fig. 2). Additionally, CO_{2bio} concentrations were calculated for Xi'an. They ranged from −11.3 ± 10.0 ppm (July 2013) to 51.6 ± 35.6 ppm (October 2015), with an average of 10.6 ± 11.6 ppm. Generally, the CO_{2bio} showed low values in summer and high values in autumn.

3.3. Source apportionment of CO_{2ff} during wintertime in Xi'an

We take the observed winter data of 2014 in Xi'an as an example to perform source apportionment, due to the high values during the wintertime as well as the weak photosynthesis in that season to avoid fluxes of opposing sign (Miller and Tans, 2003). Firstly, the $\delta^{13}Cs$ value from Miller-Tans regressions for winter in Xi'an was −25.6‰, which represents the weighted average contributions from fossil fuel and biosphere sources. Secondly, based on the $\Delta^{14}CO_2$ and atmospheric CO_2 data, the contributions of fossil fuel and biosphere sources (including plant and soil respiration, biofuel and human respiration) were 92.7 ± 9.7% and 7.3 ± 9.7% of the atmospheric CO_2 offsets over background CO_2 concentrations, respectively (Fig. 3). Thirdly, a value of −26.7‰ was obtained for $\delta^{13}C_{ff}$ by the Eq. (8). Finally, according to the Eqs.(9) and (10) and statistics data for natural gas mentioned

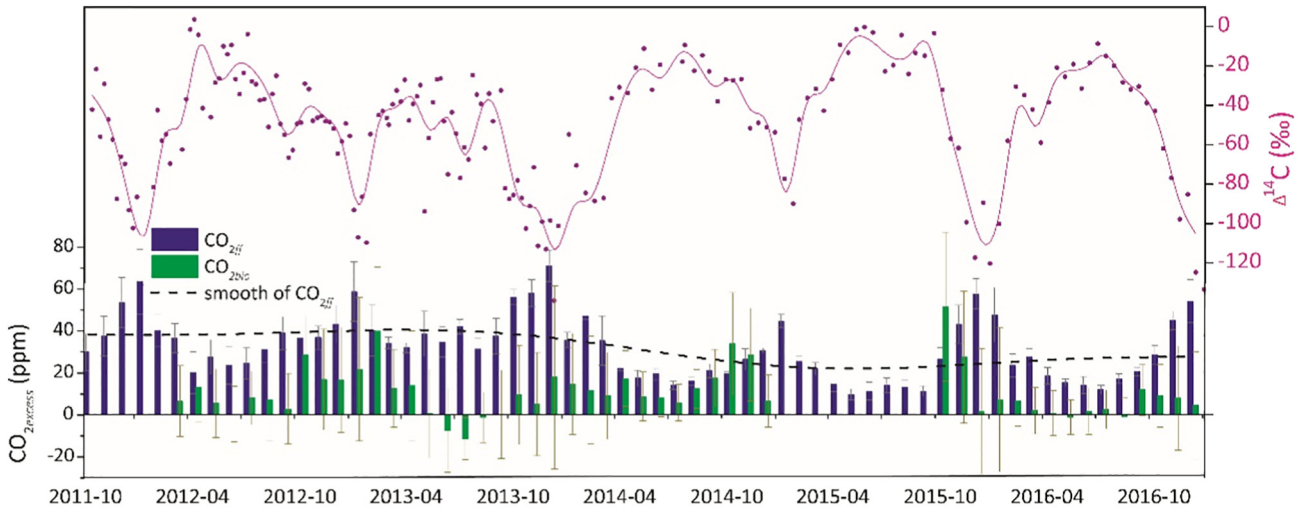

Fig. 2. $\Delta^{14}CO_2$ (red dots), CO_{2ff} (blue bars) and CO_{2bio} (green bars) variations in Xi'an during 2011/10–2016/12. The solid and dashed lines are Fourier Transform-smoothed (period of 6 data points) for $\Delta^{14}CO_2$ and CO_{2ff}, respectively. There are no CO_{2bio} data from January to September 2015 due to an equipment malfunction.

above, the contributions of coal combustion and vehicle exhaust to CO_{2ff} were 72.6 ± 10.4% and 13.8 ± 10.4%, respectively (Fig. 3).

To assess the uncertainties in partitioning resulted from variations in $\delta^{13}C$ end members (fossil fuel sources), a series of sensitivity analyses were conducted. It was found that a 1‰ depletion in natural gas and vehicle exhaust generally caused a 1.7% increase in the contribution of coal burning and a 1.7% decrease in the contribution of vehicle exhaust. A 1‰ depletion in the $\delta^{13}C$ of coal caused a 10.8% increase in the contribution of coal burning, but the $\delta^{13}C$ of coal is relatively stable (−23.5 ± 0.5‰) (Tang, 2001). It should be noted that the proportion of natural gas used in Eqs.(9, 10) represents the annual average. Considering there is more coal and natural gas consumption in winter for residential heating, natural gas emissions are likely to be higher than the annual average during wintertime. Our source apportionment showed that the increment in natural gas emissions generally caused the increase in coal emissions. Thus, the actual contributions of coal and natural gas sources might be higher than our source apportionment results in wintertime.

These results differ from some cities in developed countries which have higher proportions of gasoline and natural gas in fossil fuel consumption compared to Xi'an. For example, a study carried out in the megacity of Los Angeles showed contributions of petroleum and natural gas burning, to excess CO_2, are 68% and 32% during the cooler months (Newman et al., 2016). In Paris, France, the liquid and gas fuel contributions are 30% and 70% to the fossil fuel emissions, respectively (Lopez et al., 2013). It is worth noting that these differences are due to the differences in energy structure between China and developed countries. Some studies ignore coal combustion, because it is documented that there is no coal burning in those regions, such as Los Angeles, CA (Newman et al., 2016). However, although there is a downward trend in coal consumption due to the economic development and energy structure adjustment in recent years (NBSC, 2017), coal is still the major fossil fuel energy source in China, especially in northern cities which consume substantial amounts of coal for heating during the winter. Since the net carbon content of raw coal (26.4 tC/TJ) is higher than oil (20.0 tC/TJ) and natural gas (15.3 tC/TJ) (Li et al., 2010), some adjustment policies in energy structure, such as the switch from coal to natural gas, will help to mitigate CO_{2ff} emissions in China.

3.4. Local or transported CO_{2ff} in Xi'an

Model simulations showed that local CO_{2ff} sources dominate wintertime CO_{2ff} concentrations in Xi'an and the greater Guanzhong region, a closed topographic basin. The Guanzhong basin has an area of about 20,000 km^2 and follows the Wei River from west to east. The model results illustrated in Fig. 4, show averaged CO_{2ff} concentrations around Xi'an in January 2014; without and with local inputs (Fig. 4a, b). It is clear from the figure that although regional transport contributes 4–8 ppm in the central and eastern Guanzhong basin, local inputs

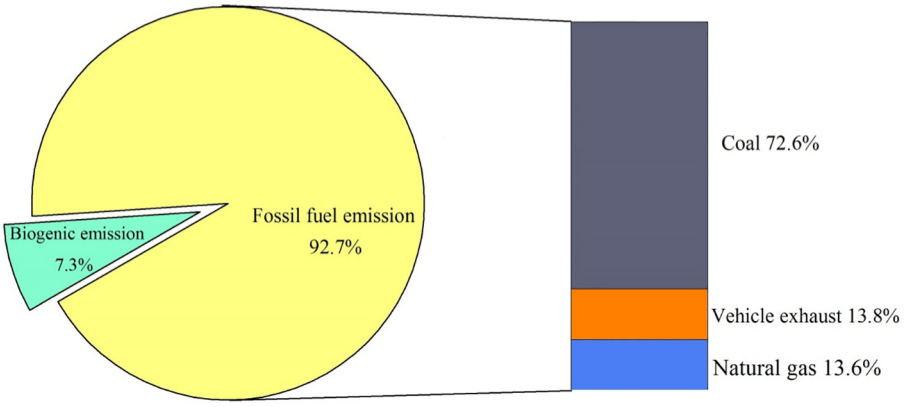

Fig. 3. The contributions of different sources to atmospheric CO_2 during wintertime 2014 in Xi'an. The pie chart represents the contributions of fossil fuel and biogenic sources to atmospheric CO_2 offset over background CO_2 concentration. The stacked column shows the contributions of different fossil fuel sources.

control the wintertime regional CO_{2ff} distribution. From the source apportionment and model results, it can be seen that reduction of coal consumption should be a primary goal for inland cities located in topographic basins to control CO_{2ff} concentrations.

3.5. Spatial-temporal variations in $\Delta^{14}CO_2$ and CO_{2ff} in Chinese cities

The average $\Delta^{14}C$ in sampling cities for January and July from 2014 to 2016 are shown in Fig. S1. The $\Delta^{14}C$ values of January samples were generally lower than those of July samples with the exception of Baoting. The $\Delta^{14}C$ differences between northern and southern metropolises in January were higher than those in July. The CO_{2ff} for each city was calculated from Eq. (4). The January CO_{2ff} values were significantly ($p < 0.01$) higher than those in July in most cities, with the exception in Baoting (Fig. 5a). The relatively high values in January in northern metropolises resulted from a shallow atmospheric boundary layer and high fossil fuel consumption for heating, and the high values in January in southern metropolises resulted from a shallow atmospheric boundary layer. Baoting is located in the tropics, with low seasonality. Relatively high CO_{2ff} concentrations were observed in the northwestern cities of Urumqi (54.7 ± 2.0 ppm), Lanzhou (42.6 ± 5.9 ppm), and Xi'an (41.6 ± 2.7 ppm) as well as in Wuhan (41.6 ± 5.6 ppm) in January, which might result from the winter heating and the disadvantageous topography. The metropolises with closed and semi-enclosed topographic basins generally showed relatively high averages of CO_{2ff} concentration, such as Urumqi (36.4 ± 3.2 ppm), Lanzhou (30.2 ± 3.4 ppm), Xi'an (28.5 ± 3.6 ppm), Wuhan (27.4 ± 3.8 ppm), Beijing (27.0 ± 0.3 ppm), and Chongqing (25.3 ± 2.1 ppm), while the metropolises with open topographic settings generally showed relatively low CO_{2ff} concentration, such as Guiyang (16.6 ± 1.5 ppm) and Harbin (15.8 ± 2.0 ppm).

CO_{2bio} concentrations in January were obviously higher than those in July for most cities (Fig. 5b), and a few negative CO_{2bio} values in July might be due to uptake by vegetation. The high CO_{2bio} in January might be related to the heterotrophic respiration, biomass burning and the weak photosynthesis during the wintertime. We inferred that the extremely high CO_{2bio} concentrations in January in Urumqi and Chongqing are likely related to biomass burning. A study concerning atmospheric particulates in Chongqing in winter 2014–2015 showed that 92.5% particulates came from biomass burning associated with seasonal meat smoking activities (Chen et al., 2017).

3.6. Correlations between CO_{2ff} and $PM_{2.5}$ in Chinese cities

The correlations of $PM_{2.5}$ and CO_{2ff} were investigated for each city. Interestingly, significant ($p < 0.01$) correlations (Table 2) are found between $PM_{2.5}$ and CO_{2ff} in most of the studied Chinese cities, and this correlation is observed in a variety of topographic settings, from a basin (Xi'an), a semi-enclosed basin (Beijing) to an open topographic environment (Shanghai), indicating the universality of the correlations in Chinese cities. We found severe haze episodes in these cities often accompany high CO_{2ff} concentrations. The correlations resulted from the common sources of CO_{2ff} and some constituents of $PM_{2.5}$. The *Action Plan* instituted in September 2013 was primarily designed to decrease $PM_{2.5}$, but also influenced CO_{2ff} concentrations, for example, the measure of replacing coal with natural gas. Taking Xi'an as an example, the annual averages of $PM_{2.5}$ concentrations decreased from ca.123.5 ± 9.5 μg m^{-3} during 2011–2013 (Cheng et al., 2014; Huang et al., 2015) to 69.6 ± 8.4 μg m^{-3} during 2014–2016 (China MEP, 2016), and the annual averages of CO_{2ff} concentrations decreased from 40.1 ± 3.8 ppm to 25.7 ± 1.1 ppm (a decrease of 35.9 ± 6.6%). The ratio of $PM_{2.5}$:CO_{2ff} (3.08) during 2011–2013 was similar to the ratio observed during 2014–2016 (2.71), indicating that $PM_{2.5}$ and CO_{2ff} could share a common source in Xi'an. Thus, the pollution control measures of the *Action Plan* produced decreases in both $PM_{2.5}$ and CO_{2ff} concentrations in Chinese cities.

The slope of the regression line between $PM_{2.5}$ and CO_{2ff} is, in part, a function of the type of fossil fuel utilized. A high slope is expected in the case of coal combustion, as the particulate load associated with coal combustion is known to be high (Andersson et al., 2015; Zhang et al., 2015). For cities with high slopes, coal remains the primary fossil fuel, as showed by our source apportionment analysis for Xi'an. In Chongqing and Harbin, the ratios of coal usages are ca. 65% and 73%, respectively (CMBS, 2016; HMBS, 2016). Low slopes would result from higher proportions of cleaner fossil fuels, such as natural gas. For example, the city of Xining, with a relatively high (26%) ratio of natural gas consumption shows relatively low slope (QPBS, 2016), and Beijing also shows a relatively low slope with a relatively high (37.2%) ratio of natural gas

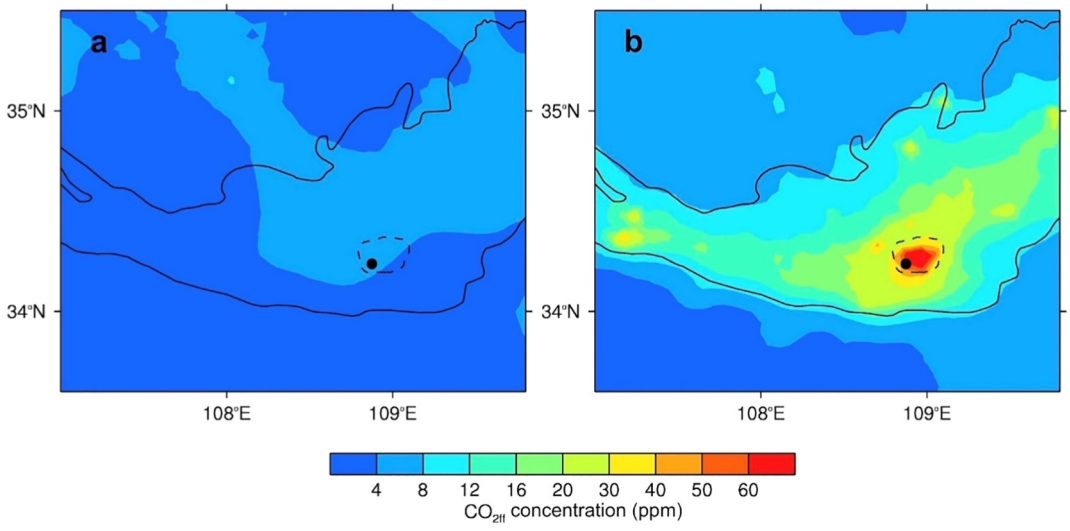

Fig. 4. Spatial distributions of simulated CO_{2ff} concentrations in the Guanzhong basin in January 2014 without (a) and with (b) local CO_{2ff} emissions. The black dot indicates the location of the CO_2 measurements. The red zone is centered on Xi'an. The dashed line shows the position of the outermost ring road in Xi'an. The black curves show the 1000-m topographic contour along the Chinese Loess Plateau to the north, and Qinling Mountains to the south, indicating the area of the Guanzhong basin. The atmospheric mixing of CO_{2ff} is simulated with a modified WRF-CHEM model, using the data of Zhang et al. (2009) to quantify CO_{2ff} sources.

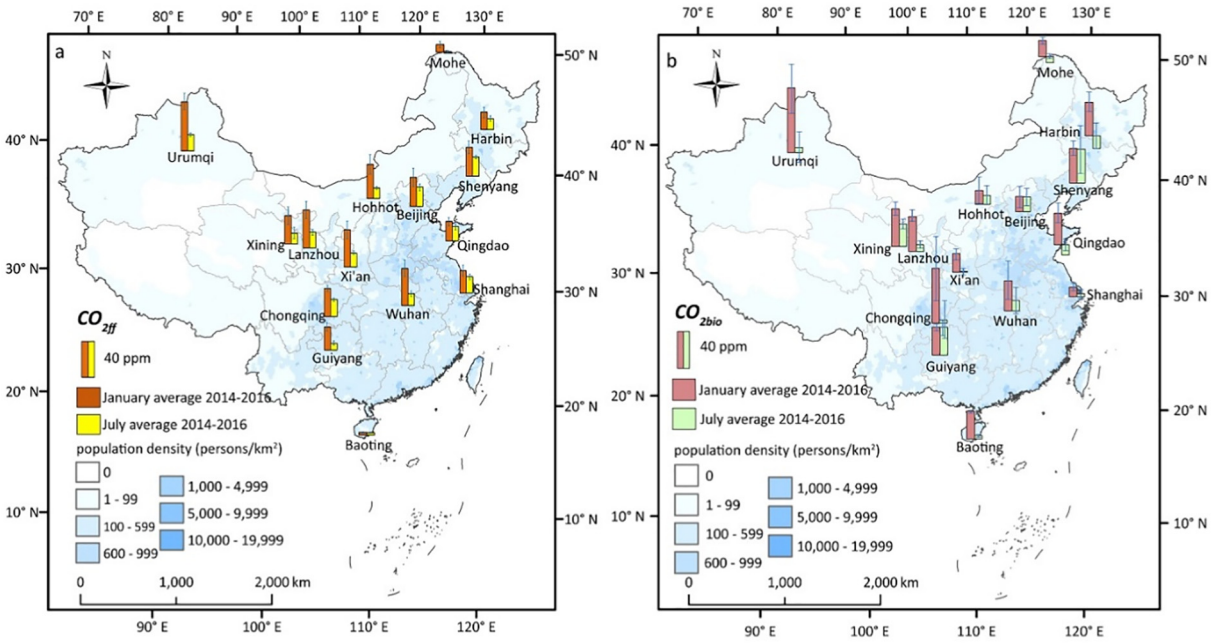

Fig. 5. Average CO_{2ff} (a) and CO_{2bio} (b) concentrations in January (brown bar and red bar) and July (yellow bar and greed bar) during 2014–2016 in Chinese cities. The depth of blue in China map reflects population density.

consumption and low ratio (17.9%) of coal consumption (BMBS, 2016). Thus, for the cities with a strong correlation coefficient and high slope between $PM_{2.5}$ and CO_{2ff}, reduction of coal usage, especially during wintertime, should prove to be an effective means of reducing $PM_{2.5}$ and CO_{2ff}.

4. Conclusions

Significant ($p < 0.01$) correlations were found between $PM_{2.5}$ and CO_{2ff} in most of the Chinese cities. Reductions in both CO_{2ff} and $PM_{2.5}$ concentrations in Xi'an were observed from 2011 to 2016. These decreases are ascribed to governmental air pollution guidelines adopted from the *Action Plan on Prevention and Control of Air Pollution*. Although the Action Plan was designed to control $PM_{2.5}$, it also curtails CO_{2ff} emissions.

Distinct seasonality in CO_{2ff} concentrations were found from nearly all mainland Chinese cities, with high values in January, especially in the northwest. Broad topographic control on CO_{2ff} concentrations was identified. Metropolises located in closed and semi-enclosed topography generally show enhanced CO_{2ff} concentrations. For such cities, reduction of local coal consumption is an especially important pollution control step. This conclusion is supported by modeling experiments in Xi'an, which show that most of the wintertime CO_{2ff} comes from local sources.

Table 2
Correlations between $PM_{2.5}$ and CO_{2ff} in 13 Chinese metropolises.

City	Correlation coefficient (R)	Significance	Slope ($\mu g/m^3 \cdot ppm^{-1}$)
Harbin	\	<0.01	3.23
Urumqi	0.829	<0.01	3.17
Shenyang	0.535	<0.01	2.21
Hohhot	0.414	<0.01	1.35
Beijing	0.828	<0.01	1.45
Xining	0.659	<0.01	0.51
Qingdao	0.716	<0.01	2.66
Lanzhou	0.737	<0.01	0.46
Xi'an	0.738	<0.01	2.23
Shanghai	0.766	<0.01	2.12
Wuhan	0.824	<0.01	2.68
Chongqing	0.837	<0.01	3.98
Guiyang	0.635	<0.01	0.75

Note: correlation analyses are not conducted for Baoting and Mohe, because there are no $PM_{2.5}$ data available for the two small counties in China.

CRediT authorship contribution statement

Weijian Zhou: Conceptualization, Investigation, Formal analysis, Writing - review & editing.**Zhenchuan Niu:**Formal analysis.**Shugang Wu:**Investigation, Formal analysis, Writing - review & editing.**Xiaohu Xiong:**Investigation, Formal analysis, Writing - review & editing.**Yaoyao Hou:**Investigation, Formal analysis, Writing - review & editing.**Peng Wang:**Investigation, Formal analysis, Writing - review & editing.**Tian Feng:**Investigation, Formal analysis, Writing - review & editing.**Peng Cheng:**Investigation, Formal analysis, Writing - review & editing.**Hua Du:**Investigation, Formal analysis, Writing - review & editing.**Xuefeng Lu:**ormal analysis**Zhisheng An:**Writing - review & editing.**G.S. Burr:** Writing - review & editing.**Yizhi Zhu:**Investigation, Formal analysis, Writing - review & editing.

Declaration of competing interest

The authors declare no conflict of interest.

Acknowledgments

This work was jointly supported by National Science Foundation of China (41730108, 41773141, and 41573136), the Strategic Priority Research Program of the Chinese Academy of Sciences (XDB40010100, XDA23010302), National Research Program for Key Issues in Air Pollution Control (DQGG0105-02), Natural Science Basic Research Program of Shaanxi (2019JCW-20), the Youth Innovation Promotion Association CAS (2016360), and Chinese Academy of Sciences. The anonymous reviewers are acknowledged for their valuable comments.

Appendix A. Supplementary data

Supplementary data to this article can be found online at https://doi.org/10.1016/j.scitotenv.2020.138639.

References

Andersson, A., Deng, J., Du, K., Zheng, M., Yan, C., Sköld, M., Gustafsson, Ö., 2015. Regionally-varying combustion sources of the January 2013 severe haze events over eastern China. Environ. Sci. Technol. 49, 2038–2043.

Bakwin, P.S., Tans, P.P., White, J.W.C., 1998. Determination of the isotopic ($^{13}C/^{12}C$) discrimination by terrestrial biology from a global network of observations. Glob. Biogeochem. Cycles 12, 555–562.

Beijing Municipal Bureau of Statistics (BMBS), 2016. Beijing Statistical Yearbook. China Statistics Press, Beijing, China, p. 2016.

Boden, T.A., Marland, G., Andres, R.J., 2013. Global, Regional, and National Fossil-Fuel CO_2 Emissions. Oak Ridge National Laboratory, US Department of Energy.

BP, 2018. Statistical Review of World Energy 2018.

Chen, F., Dudhia, J., 2001. Coupling an advanced land surface-hydrology model with the Penn State-NCAR MM5 modeling system. Part II: preliminary model validation. Mon. Weather Rev. 129, 569–585.

Chen, Y., Wenger, J.C., Yang, F., Cao, J., Huang, R., Shi, G., Zhang, S., Tian, M., Wang, H., 2017. Source characterization of urban particles from meat smoking activities in Chongqing, China using single particle aerosol mass spectrometry. Environ. Pollut. 228, 92–101.

Cheng, Y., Fan, W., Liu, S., Xiao, B., Guo, W., Li, W., Wang, N., 2014. Characteristics of $PM_{2.5}$ and carbonaceous aerosols in Xi'an. Xi'an Univ. of Arch. & Tech. 46, 888–893 (in Chinese).

Chinese State Council, 2013. Atmospheric pollution prevention and control action plan. Retrieved from. http://www.gov.cn/zwgk/2013-09/12/content_2486773.htm.

Chongqing Municipal Bureau of Statistics (CMBS), 2016. Chongqing Statistical Yearbook. China Statistics Press, Beijing, China, p. 2016.

Chou, M., Suarez, M.J., Liang, X., Yan, M.M.-H., Cote, C., 2001. A thermal infrared radiation parameterization for atmospheric studies. NASA Tech. Rep. 19, 1–55.

Chou, M.-D., Suarez, M.J., 1999. A solar radiation parameterization for atmospheric studies (No. NASA/TM-1999- 10460)" NASA Technique Report.

Clark-Thorne, S.T., Yapp, C.J., 2003. Stable carbon isotope constraints on mixing and mass balance of CO_2 in an urban atmosphere: Dallas metropolitan area, Texas. USA. Appl. Geochem. 18, 75–95.

Coplen, T.B., 1995. Discontinuance of SMOW and PDB. Nature 375, 285.

Dhakal, S., 2009. Urban energy use and carbon emissions from cities in China and policy implications. Energy Policy 37, 4208–4219.

Djuricin, S., Pataki, D.E., Xu, X., 2010. A comparison of tracer methods for quantifying CO_2 sources in an urban region. J. Geophys. Res. 115, D11303.

Feng, T., Li, G., Cao, J., Bei, N., Shen, Z., Zhou, W., Liu, S., Zhang, T., Wang, Y., Huang, R.-J., Tie, X., Molina, L.T., 2016. Simulations of organic aerosol concentrations during springtime in the Guanzhong Basin, China. Atmos. Chem. Phys. 16, 10045–10061.

Feng, T., Zhou, W.J., Wu, S.G., Niu, Z.C., Cheng, P., Xiong, X.H., Li, G.H., 2018. Simulations of summertime fossil fuel CO_2 in the Guanzhong basin, China. Sci. Total. Environ. 624, 1163–1170.

GMD-ESRL, 2014. Global Monitoring Division of the Earth System Research Laboratory. National Oceanic and Atmospheric Administration, U.S. Department of Commerce (Retrieved from ftp://aftp.cmdl.noaa.gov/data/trace_gases/co2/flask/surface/co2_wlg_surface-flask_1_ccgg_month.txt). ftp://aftp.cmdl.noaa.gov/data/trace_gases/co2c13/flask/surface/co2c13_wlg_surface-flask_1_sil_month.txt.

Godwin, H., 1962. Half-life of radiocarbon. Nature 195, 984.

Graven, H.D., Gruber, N., 2011. Continental-scale enrichment of atmospheric $^{14}CO_2$ from the nuclear power industry: potential impact on the estimation of fossil fuel-derived CO_2. Atmos. Chem. Phys. 11, 12339–12349.

Hammer, S., Levin, I., 2017. Monthly Mean Atmospheric $\Delta^{14}CO_2$ at Jungfraujoch and Schauinsland From 1986 to 2016. heiDATA, p. V2.

Harbin Municipal Bureau of Statistics (HMBS), 2016. Harbin Statistical Yearbook. China Statistics Press, Beijing, China, p. 2016.

Huang, P., Zhang, J., Tang, Y., Liu, L., 2015. Spatial and temporal distribution of $PM_{2.5}$ pollution in Xi'an city, China. Int. J. Environ. Res. Public Health 12, 6608–6625.

Janjić, Z.I., 2002. Nonsingular Implementation of the Mellor-Yamada Level 2.5 Scheme in the NCEP Meso Model. NCEP office note.

Levin, I., Kromer, B., 2004. The tropospheric $^{14}CO_2$ level in mid-latitudes of the Northern Hemisphere (1959–2003). Radiocarbon 46, 1261–1272.

Levin, I., Kromer, B., Schmidt, M., Sartorius, H., 2003. A novel approach for independent budgeting of fossil fuels CO_2 over Europe by $^{14}CO_2$ observations. Geophys. Res. Lett. 30, 2194.

Levin, I., Naegler, T., Kromer, B., Diehl, M., Francey, R.J., Gomez-Pelaez, A.J., Steele, L.P., Wagenbach, D., Weller, R., Worthy, D., 2010. Observations and modelling of the global distribution and long-term trend of atmospheric $^{14}CO_2$. Tellus B 62, 26–46.

Levin, I., Kromer, B., Hammer, S., 2013. Atmospheric $\Delta^{14}CO_2$ trend in Western European background air from 2000 to 2012. Tellus B 65, 20092.

Li, G., Zavala, M., Lei, W., Tsimpidi, A.P., Karydis, V.A., Pandis, S.N., Canagaratna, M.R., Molina, L.T., 2011. Simulations of organic aerosol concentrations in Mexico City using the WRF-CHEM model during the MCMA-2006/MILAGRO campaign. Atmos. Chem. Phys. 11, 3789–3809. https://doi.org/10.5194/acp-11-3789-2011.

Li, L., Chen, C., Xie, S., Huang, C., Cheng, Z., Wang, H., Wang, Y., Huang, H., Lu, J., Dhakal, S., 2010. Energy demand and carbon emissions under different development scenarios for Shanghai, China. Energy Policy 38, 4797–4807.

Li, M., Zhang, Q., Kurokawa, J.-I., Woo, J.-H., He, K., Lu, Z., Ohara, T., Song, Y., Streets, D.G., Carmichael, G.R., Cheng, Y., Hong, C., Huo, H., Jiang, X., Kang, S., Liu, F., Su, H., Zheng, B., 2017. MIX: a mosaic Asian anthropogenic emission inventory under the international collaboration framework of the MICS-Asia and HTAP. Atmos. Chem. Phys. 17, 935–963.

Lin, Y., Farley, R.D., Orville, H.D., 1983. Bulk parameterization of the snow field in a cloud model. J. Clim. Appl. Meteorol. 22, 1065–1092.

Liu, Z., Guan, D., Wei, W., Davis, S.J., Ciais, P., Bai, J., Peng, S., Zhang, Q., Hubacek, K., Marland, J., Andres, R.J., Crawford-Brown, D., Lin, J., Zhao, H., Hong, C., Boden, T.A., Feng, K., Peters, G.P., Xi, F., Liu, J., Li, Y., Zhao, Y., Zeng, N., He, K., 2015. Reduced carbon emission estimates from fossil fuel combustion and cement production in China. Nature 524, 335–338.

Lopez, M., Schmidt, M., Delmotte, M., Colomb, A., Gros, V., Janssen, C., Lehman, S.J., Mondelain, D., Perrussel, O., Ramonet, M., Xueref-Remy, I., Bousquet, P., 2013. NOx and $^{13}CO_2$ as tracers for fossil fuel CO_2: results from a pilot study in Paris during winter 2010. Atmos. Chem. Phys. 13, 7343–7358.

Miller, J.B., Tans, P.P., 2003. Calculating isotopic fractionation from atmospheric measurements at various scales. Tellus B 55, 207–214.

Ministry of Environment Protection (MEP), China, 2016. Online monitoring and analysis platform of China air quality. http://www.aqistudy.cn.

Moore, J., Jacobson, A.D., 2015. Seasonally varying contributions to urban CO_2 in the Chicago, Illinois, USA region: Insights from a high-resolution CO_2 concentration and $\delta^{13}C$ record. Elem Sci Anth 3, 000052.

National Bureau of Statistics of China (NBSC), 2017. China Statistical Yearbook, 2017.

Newman, S., Xu, X.M., Gurney, K.R., Hsu, Y.K., Li, K.F., Jiang, X., Keeling, R., Feng, S., O'Keefe, D., Patarasuk, R., Wong, W.K., Rao, P., Fischer, M.L., Yung, Y.L., 2016. Toward consistency between trends in bottom-up CO_2 emissions and top-down atmospheric measurements in the Los Angeles megacity. Atmos. Chem. Phys. 16, 3843–3863.

Niu, Z.C., Zhou, W.J., Wu, S.G., Cheng, P., Lu, X.F., Xiong, X.H., Du, H., Fu, Y.C., 2016. Atmospheric fossil fuel CO_2 traced by $\Delta^{14}C$ in Beijing and Xiamen, China: temporal variations, inland/coastal differences and influencing factors. Environ. Sci. Technol. 50, 5474–5480.

Pang, J., Wen, X., Sun, X., 2016. Mixing ratio and carbon isotopic composition investigation of atmospheric CO_2 in Beijing, China. Sci. Total Environ. 539, 322–330.

Pataki, D.E., Bowling, D.R., Ehleringer, J.R., 2003. Seasonal cycle of carbon dioxide and its isotopic composition in an urban atmosphere: anthropogenic and biogenic effects. J. Geophys. Res. 108, D23.

Qinghai Provincial Bureau of Statistics (QPBS), 2016. Qinghai Statistical Yearbook. China Statistics Press, Beijing, China, p. 2016.

Randerson, J.T., van der Werf, G.R., Giglio, L., Collatz, G.J., Kasibhatla, P.S., 2018. Global Fire Emissions Database, Version 4. ORNL DAAC, Oak Ridge, Tennessee, USA.

Rödenbeck, C., Houweling, S., Gloor, M., Heimann, M., 2003. CO_2 flux history 1982–2001 inferred from atmospheric data using a global inversion of atmospheric transport. Atmos. Chem. Phys. 3, 1919–1964.

Shan, Y., Guan, D., Liu, J., Mi, Z., Liu, Z., Liu, J., Schroeder, H., Cai, B., Chen, Y., Shao, S., Zhang, Q., 2017. Methodology and applications of city level CO_2 emission accounts in China. J. Clean. Prod. 161, 1215–1225.

Slota, P., Jull, A.T., Linick, T., Toolin, L., 1987. Preparation of small samples for ^{14}C accelerator targets by catalytic reduction of CO. Radiocarbon 29, 303–306.

Stuiver, M., Polach, H., 1977. Discussion: reporting of ^{14}C data. Radiocarbon 3, 355–363.

Takahashi, H.A., Konohira, E., Hiyama, T., Minami, M., Nakamura, T., Yoshida, N., 2002. Diurnal variation of CO_2 concentration, $\Delta^{14}C$ and $\delta^{13}C$ in an urban forest: estimate of the anthropogenic and biogenic CO_2 contributions. Tellus 54B, 97–109.

Tang, G., 2001. $\delta^{13}C$ Characteristics of Carboniferous Coal in North China and Its Paleo Geographic Implications, (Political Scholars Anthology of Peking University). Peking University, Beijing.

Tie, X., Wu, D., Brasseur, G., 2009. Lung cancer mortality and exposure to atmospheric aerosol particles in Guangzhou, China. Atmos. Environ. 43, 2375–2377.

Turnbull, J., Rayner, P., Miller, J., Naegler, T., Ciais, P., Cozic, A., 2009. On the use of $^{14}CO_2$ as a tracer for fossil fuel CO_2: quantifying uncertainties using an atmospheric transport model. J. Geophys. Res. 114, 1–13.

Turnbull, J.C., Miller, J.B., Lehman, S.J., Tans, P.P., Sparks, R.J., Southon, J., 2006. Comparison of $^{14}CO_2$, CO, and SF_6 as tracers for recently added fossil fuel CO_2 in the atmosphere and implications for biological CO_2 exchange. Geophys. Res. Lett. 33, 1–5.

United Nations (UN), 2014. Department of Economic and Social Affairs, Population Division. World Urbanization Prospects: The 2014 Revision. CD-ROM edition. .

Vogel, F.R., Levin, I., Worthy, D.E.J., 2013. Implications for deriving regional fossil fuel CO_2 estimates from atmospheric observations in a hot spot of nuclear power plant $^{14}CO_2$ emissions. Radiocarbon 55 (2–3), 1556–1572.

Willmott, C.J., 1981. On the Validation of Models. Phys. Geogr. 2, 184–194. https://doi.org/10.1080/02723646.1981.10642213.

Xi, X.T., Ding, X.F., Fu, D.P., Zhou, L.P., Liu, K.X., 2011. Regional $\Delta^{14}C$ patterns and fossil fuel derived CO_2 distribution in the Beijing area using annual plants. Chin. Sci. Bull. 56, 1721–1726.

Xi"an Municipal Bureau of Statistics (XMBS), 2017. Xi'an Statistical Yearbook. China Statistics Press, Beijing.

Zhang, Q., Streets, D.G., Carmichael, G.R., He, K.B., Huo, H., Kannari, A., Klimont, A., Park, I.S., Reddy, S., Fu, J.S., Chen, D., Duan, L., Lei, Y., Wang, L.T., Yao, Z.L., 2009. Asian emissions in 2006 for the NASA INTEX-B mission. Atmos. Chem. Phys. 9, 5131–5153.

Zhang, Y., Huang, R., El Haddad, I., Ho, K., Cao, J., Han, Y., Zotter, P., Bozzetti, C., Daellenbach, K.R., Canonaco, F., Slowik, J.G., Salazar, G., Schwikowski, M., Schnelle-Kreis, J., Abbaszade, G., Zimmermann, R., Baltensperger, U., Prévôt, A.S.H., Szidat, S., 2015. Fossil vs. non-fossil sources of fine carbonaceous aerosols in four Chinese cities during the extreme winter haze episode of 2013. Atmos. Chem. Phys. 15 (3), 1299–1312.

Zhou, W.J., Zhao, X.L., Lu, X.F., Liu, L., Wu, Z.K., Cheng, P., Zhao, W.N., Huang, C.H., 2006. The 3MV multi-element AMS in Xi'an, China: unique features and preliminary test. Radiocarbon 48, 285–293.

Zhou, W.J., Wu, S.G., Huo, W.W., Xiong, X.H., Cheng, P., Lu, X.F., Niu, Z.C., 2014. Tracing fossil fuel CO_2 using $\Delta^{14}C$ in Xi'an City, China. Atmos. Environ. 94, 538–545.

Zondervan, A., Meijer, H.A.J., 1996. Isotopic characterisation of CO_2 sources during regional pollution events using isotopic and radiocarbon analysis. Tellus B 48, 601–612.